ISPRS Journal of Photogrammetry and Remote Sensing 158 (2019) 90–98

Contents lists available at ScienceDirect

ISPRS Journal of Photogrammetry and Remote Sensing

journal homepage: www.elsevier.com/locate/isprsjprs

Quantifying $PM_{2.5}$ mass concentration and particle radius using satellite data and an optical-mass conversion algorithm

Ming Liu[a], Gaoxiang Zhou[a,b], Rebecca K. Saari[c], Sabrina Li[d], Xiangnan Liu[b], Jonathan Li[a,*]

[a] Department of Geography and Environmental Management, University of Waterloo, Waterloo, Ontario N2L 3G1, Canada
[b] School of Information Engineering, China University of Geosciences, Beijing 100083, China
[c] Department of Civil and Environmental Engineering, University of Waterloo, Waterloo, Ontario N2L 3G1, Canada
[d] School of Geography and the Environment, University of Oxford, Oxford OX1 2JD, United Kingdom

ARTICLE INFO

Keywords:
$PM_{2.5}$
Particle radius
Aerosol optical depth
MODIS
China

ABSTRACT

Although satellite-based approaches have been developed and adopted for estimating the concentration of fine particulate matter ($PM_{2.5}$) with promising accuracy, few studies have considered mass concentration and particle radius simultaneously, even though particle size is significant for human health impacts. We developed a satellite-based $PM_{2.5}$ retrieval method using optical-mass relationships via aerosol microphysical characteristics. Satellite data from the MODerate resolution Imaging Spectroradiometer (MODIS) instrument, combined with parameters from meteorological reanalysis, were processed to calculate particle radii and retrieve $PM_{2.5}$ mass concentrations over China in 2017. Our study is the first to identify the spatial pattern of mean $PM_{2.5}$ radius over China, which was validated against observations from AERONET (RMSE = 0.11 μm). Mean particle size over eastern China is smaller than in the west, depicting a clear bifurcation across the country, especially in summertime. This finding is attributed to variations in topography, meteorology, land use and population density, which affects the properties of emitted aerosols as well as their fate and transport. A statistically significant correlation (R = 0.82) was observed between estimated and measured annual $PM_{2.5}$, with RMSE = 9.25 μg/m^3, MAE = 6.98 μg/m^3, MBE = −1.98 μg/m^3 and RPE = 17.69% (N = 1270). The spatiotemporal distributions of resulting $PM_{2.5}$ are consistent with previous findings, indicating the effectiveness and applicability of our method. Our approach quantifies $PM_{2.5}$ mass concentrations without introducing regionally-specific fitting parameters, which can be efficiently applied across various spatial and temporal domains.

1. Introduction

Suspended particulate matter with aerodynamic diameter less than 2.5 μm ($PM_{2.5}$) poses a serious threat to public health through increased risks to mortality, cardiovascular, and respiratory illnesses, among others (de Hartog et al., 2009; Sacks et al., 2011; Pope et al., 2018;). It is the single greatest global environmental health risk factor identified in the Global Burden of Disease (Cohen et al., 2017). China has experienced severe $PM_{2.5}$ pollution with its recent economic and industrial development. Since 2013, the Chinese government has released air pollutant concentrations to the public. More than 1400 stations provide hourly $PM_{2.5}$ concentrations, which makes $PM_{2.5}$ retrieval and validation feasible (Lin et al., 2015). However, a fixed-site monitoring network restricts the spatial resolution and coverage of pollutant measurements for the benefit of high accuracy and temporal resolution. In order to obtain the spatial coverage required for full country-level exposure estimates, satellite remote sensing techniques are increasingly indispensable in studies of $PM_{2.5}$.

Aerosol optical depth (AOD) observed by satellites is closely associated with $PM_{2.5}$ and often employed to retrieve mass concentrations (You et al., 2015). There are two main methods employed for satellite-based $PM_{2.5}$ retrieval: data-driven methods and process-driven methods, each with advantages and limitations. Data-driven models developed including statistical or artificial intelligence methods have been applied to derive quantitative AOD-$PM_{2.5}$ relationships. Examples include general linear regression models (Kumar et al., 2007; Liu et al., 2005), mixed effects models (Hu et al., 2014; Lee et al., 2011), generalized additive models (Liu et al., 2012; Liu et al., 2009), land use regression models (Di et al., 2016; Yang et al., 2017), geographical weighted regression models (Li et al., 2017; Luo et al., 2017; Yao et al., 2019; You et al., 2016) and artificial neural networks (Gupta and Christopher, 2009; Zhao et al., 2016; Ma et al., 2019). In addition to

* Corresponding author.
E-mail address: junli@uwaterloo.ca (J. Li).

https://doi.org/10.1016/j.isprsjprs.2019.10.010
Received 29 March 2019; Received in revised form 29 September 2019; Accepted 16 October 2019

AOD, meteorological parameters, such as planetary boundary layer height (PBLH), relative humidity (RH) and wind speed, (Guo et al., 2017a; Li et al., 2015; Zhang et al., 2015a), land use data (Chen et al., 2016; Yang et al., 2017) and socioeconomic data (Hao and Liu 2016; Lin et al., 2013) have been found to be associated with $PM_{2.5}$, and were employed as input parameters of various data-driven models (Han et al., 2016; Luo et al., 2017). Such data-driven models have performed very well in representing the variation of ground-level $PM_{2.5}$ concentrations in a specific spatial and temporal domain. However, while their predictive power is high, they do not rely explicitly on scientific relationships, which limits their interpretability. Process-driven numerical simulation models, such as chemical-transport models (CTMs), offer an alternative to obtain mass concentrations that simulate physical and chemical relationships, which afford both predictive and explanatory power (Steyn and Galmarini 2008). CTMs have been shown to simulate aerosol behavior with relatively high spatial (horizontal and vertical) and temporal resolution (Di et al., 2016; Tang et al., 2015; van Donkelaar et al., 2015). However, the accuracy of simulation results relies on emissions, atmospheric conditions (including meteorology and chemical composition), and simulated chemical and transport mechanisms.

An alternative to data-driven and numerical simulation models has been developed to achieve reasonable predictive power and add some explanatory power without the computational expense of a full numerical simulation. With this aim, several methods have been developed focusing on converting optical properties to mass (herein called "optical-mass conversion"). Lin et al. (2015) proposed an indicator describing the synthetic influence of hygroscopic growth instead of using a fixed humidity effect to estimate $PM_{2.5}$ concentration. Zhang and Li (2015) defined a "particle columnar volume-to-extinction ratio (VE_f)" to establish a $PM_{2.5}$ retrieval algorithm with satellite-derived parameters. Their studies contributed to the understanding of optical-mass physical relationships, but still relied on model fitting or statistical assumptions in the retrieval, such as the empirical relationship between fine mode fraction (FMF) and VE_f, and fitted parameters for aerosol integrated effect quantification. Additionally, inherent particle properties, such as particle radius, have not been estimated previously. Recent studies suggest that most of the health impacts of $PM_{2.5}$ are caused by particles with a radius less than 2.5 μm, such as PM_1 (Chen et al., 2017; Ostro et al., 2015; Samoli et al., 2016; Stafoggia et al., 2017). Therefore, understanding size distribution of particles at finer scales is essential for mass concentration retrieval, which then can be applied to better understand the health impacts of $PM_{2.5}$.

This study presents a $PM_{2.5}$ retrieval method with a theoretical basis using satellite observations, meteorological information and ground-level $PM_{2.5}$ measurements, which can simultaneously estimate particle radius. Mainland China is applied as the case study to quantitatively assess the performance of the proposed algorithm. The particle radius and $PM_{2.5}$ concentrations are estimated and validated with station measurements. The advantages and uncertainty of our retrieval method are also discussed.

2. Data collection

2.1. Ground measurements

Hourly average $PM_{2.5}$ observations in 2017 were obtained from the "China National Environmental Monitoring Center (CNEMC) (http://www.cnemc.cn/)". Monitoring stations are mainly situated in southeastern China, reflecting the population distribution. All measurements were calibrated and processed with quality control according to "China's National Ambient Air Quality Standards (GB3095-2012)" and "Environmental Protection Standards (HJ618-2011)" (China 2012). $PM_{2.5}$ concentration was measured by Thermo Fisher 1405 using the "Filter Dynamic Measurements System" and "Tapered Element Oscillating Microbalance". Daily $PM_{2.5}$ concentrations were calculated from hourly measurements during 10:00–14:00 local time.

The Aerosol Robotic Network (AERONET) Version 3 Level 2.0 AOD from 2013 to 2016 were downloaded from http://aeronet.gsfc.nasa.gov/ to calibrate MODIS AOD products in 2017 in order to increase the available calibration samples. AERONET AOD at 0.55 μm were interpolated by AOD at 0.44 μm, 0.67 μm and 0.87 μm, respectively. Many studies (He and Huang 2018; Yang and Hu 2018) used Angstrom's empirical expression, which is related to the Junge distribution (Junge 1955), to interpolate AOD at 550 nm. However, King and Byrne (1976) indicated that particle size distributions do not follow the Junge distribution and the radii do not extend from zero to infinity. Therefore, we employed the 2nd-order polynomial equation (Eck et al., 1999):

$$\ln\ \tau_a = a_0 + a_1 \ln\ \lambda + a_2 (\ln\ \lambda)^2 \quad (1)$$

where τ_a is AOD at the wavelength of λ. a_0, a_1 and a_2 are the coefficients, which can be fitted by the measurements.

The AERONET data within ± 30min of satellite overpass time (Terra UTC 2:00–3:00; Aqua UTC 5:00–6:00) were selected and averaged to match the pixel values of MODIS products.

2.2. Satellite data

2.2.1. MODIS

Currently, MODIS onboard the Terra and Aqua satellites provide three retrieval algorithms for aerosol properties over land globally: the "Dark Target (DT)" algorithm, the "Deep Blue (DB)" algorithm and the "Multi-Angle Implementation of Atmospheric Correction (MAIAC)" algorithm (Ceca et al., 2018; Hsu et al., 2013; Li et al., 2014; Lyapustin et al., 2018). With a resolution of 1 km, the MAIAC AOD is informative for local-scale studies. However, considering the geophysical coverage in this study, 3 km DT and 10 km DB AOD Collection 6.1 products from both Terra and Aqua were adopted for $PM_{2.5}$ retrieval.

Because of the large uncertainty of MODIS FMF products (Levy et al., 2007), fine mode fraction (FMF) retrieved by the LUT-SDA algorithm was adopted for fine mode AOD. The LUT-SDA algorithm is described and evaluated in previous studies (Yan et al., 2019; Yan et al., 2017a). The intermediate parameter, Angstrom exponent (AE), was calculated with MODIS AOD at 470 nm and 660 nm.

2.2.2. Data preprocessing

Before modelling, AOD products in 2017 were calibrated and gap-filled as depicted in the Supplemntary Material (Part 1). Five preprocessing steps were performed for AOD calibration and daily coverage improvement, following (He and Huang 2018; Ma et al., 2016). First, the relationships between MODIS AOD retrievals and AERONET AOD measurements from 2013 to 2016 were established. This timeframe was employed to establish the accuracy of MODIS AOD data due to the limited number of collocated MODIS-AERONET observations in 2017. The relationships are shown in Fig. S2, with the correlation coefficients higher than 0.91. Since this relationship shows strong seasonality (Remer et al., 2013), four linear regressions were built for each season and adopted for MODIS AOD calibration in 2017. MODIS AOD includes 3 km DT and 10 km DB products from the Terra and Aqua (Table S1). Next, the MODIS 10 km DB AOD were resampled into 3 km using the cubic convolution resampling algorithm. Then, a linear regression analysis between Terra and Aqua DT (DB) was performed and the regression coefficients obtained were employed to calculate the missing pixels in Terra DT (DB) if there are values in Aqua DT (DB), and vice versa. Furthermore, the variances per satellite per algorithm per season were calculated and used for combining AOD data with an inverse variance weighting (IVW) approach:

$$\mathrm{AOD} = \frac{AOD_{Aqua}/Var_{Aqua_s} + AOD_{Terra}/Var_{Terra_s}}{1/Var_{Aqua_s} + 1/Var_{Terra_s}} \quad (2)$$

where AOD is the satellite-combined DT/DB AOD with IVW; AOD_{Aqua}

and AOD_{Terra} are the DT/DB AOD values in Aqua and Terra after calibration and gap filling, respectively; Var_{Aqua_s} and Var_{Terra_s} are the variances of Aqua and Terra AOD in season s, respectively. Finally, satellite-combined DB AOD images were used to fill the missing pixels of satellite-combined DT images. The validation and coverage improvement results are shown in Figs. S3 and S4.

2.3. Meteorological data

Surface meteorological data, including RH, PBLH and visibility (VIS) data, were obtained from the NCEP/NCAR reanalysis dataset. The "NCEP GDAS/FNL 0.25 Degree Global Tropospheric Analyses and Forecast Grids (https://rda.ucar.edu/datasets/ds083.3/)" were downloaded for RH and PBLH, and the "NCEP ADP Global Surface Observational Weather Data (http://rda.ucar.edu/datasets/ds461.0/)" were utilized for VIS, which include more than 1500 stations over China received via the Global Telecommunication System. The NCEP dataset includes 6-hourly analysis products and the products at 12:00 were selected and used in this study.

2.4. Data integration

Both the satellite and the meteorological data were unified with respect to coordinate systems, data format, and image size. Daily VIS were interpolated using the inverse distance weighted (IDW) interpolation approach. Following the geophysical coverage of study area and spatial resolution of MODIS AOD, all meteorological data were masked by the extent of China before resampling to 3 km using the cubic convolution interpolation algorithm.

3. Methodology

3.1. Ground-level $PM_{2.5}$ retrieval

The purpose of our work is to retrieve ground-level dry $PM_{2.5}$ mass concentration with an optical-mass conversion algorithm. Several corrections and calculations were thus performed to convert satellite columnar observations into ground-level mass concentrations. The framework of this study is shown in Fig. 1.

AOD, which refers to the aerosol extinction (absorption and scattering) in the total vertical column of atmosphere, must be corrected into the extinction near the ground under dry conditions. According to previous studies (Hansen and Travis, 1974; Schuster et al., 2006), atmospheric aerosols present a bimodal distribution and the accumulation mode aerosol is superior for use in $PM_{2.5}$ retrieval. Therefore, the FMF was adopted for fine mode AOD calculation:

$$AOD_f = AOD * FMF \tag{3}$$

where AOD_f is the fine mode AOD.

According to Koelemeijer et al. (2006), both AOD and PM show negative correlations with precipitation (i.e. humidity), but the effect is stronger on AOD. Hence, it is necessary to remove the effect of humidity and boundary layer height on the PM retrieval. Fine 'meteo-scaled' optical depth, AOD_f^* is defined as:

$$AOD_f^* = \frac{AOD_f}{PBLH * f(RH)} \tag{4}$$

where f(RH) is the hygroscopic growth function, a function of relative humidity. The formulas of this function are based on three previous studies to diminish the effects of spatial heterogeneity (Supplementary Material) (Liu et al., 2008; Chen et al., 2014; Zhang et al., 2015b).

According to the physical definition of aerosol optical depth:

$$AOD_f^* = \int_0^\infty Q_{ext}\pi r^2 \frac{dN}{d\ln r} d\ \ln r \tag{5}$$

where $\frac{dN}{d\ln r}$ is the lognormal particle size distribution, which is described by Eq. (7); Q_{ext} is the extinction efficiency through the area distribution, which is defined by Eq. (8).

The lognormal particle size distribution was used for accumulation mode aerosols (Hansen and Travis, 1974):

$$\frac{dN}{d\ln r} = \frac{1}{\sqrt{2\pi}} \cdot \frac{1}{r\ \ln\ \sigma_g} \exp\left(-\frac{(\ln\ r - \ln\ r_g)^2}{2\ \ln^2 \sigma_g}\right) \tag{6}$$

where r_g is the lognormal geometric particle radius andσ_g is the geometric standard deviation. σ_g was set at 2μm, which refers to the general range (1.75–2.25) measured for different types of fine particles (Hofmann and Rosen 1983; Hobbs et al., 1991; Reid et al., 2003; Steele et al., 2006). Since the aerosol extinction properties are proportional to r^2, r_g is not the optimal parameter to represent the distribution. Therefore, the effective radius r_e (a weighted average of particle size

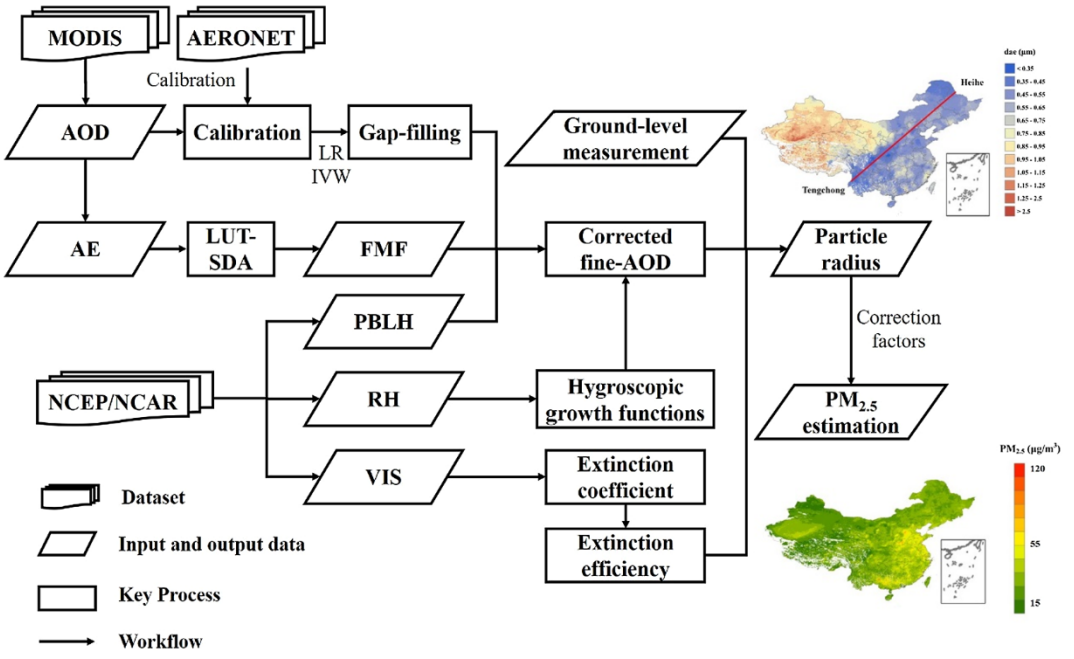

Fig. 1. The framework of $PM_{2.5}$ retrieval with optical-mass conversion algorithm.

distribution) is defined and deduced according to the rule of lognormal distribution (Hansen and Travis, 1974).

$$r_e = \frac{\int_0^\infty r^3 \frac{dN}{dlnr} d\ \ln\ r}{\int_0^\infty r^2 \frac{dN}{dlnr} d\ \ln\ r} = r_g \exp\left(\frac{5\ \ln^2\sigma_g}{2}\right) \tag{7}$$

Similarly, extinction efficiency is defined as

$$Q_{ext} = \frac{\kappa_{ext}}{\int_0^\infty \pi r^2 \frac{dN}{d\ \ln\ r} d\ \ln\ r} = \frac{\kappa_{ext}}{\pi (r_g)^2 \exp(2\ \ln^2\sigma_g)} \tag{8}$$

where κ_{ext} is the extinction coefficient, which is inversely proportional to VIS. κ_{ext} can be calculated based on the empirical relationship $\kappa_{ext} = 3.912/VIS$ (Koschmieder 1925).

Based on these definitions, fine particulate mass concentration under dry conditions at ground level can be derived as:

$$PM_f = \frac{4}{3}\pi\rho \int r^3 \frac{dN}{d\ \ln\ r} d\ \ln\ r \tag{9}$$

where PM_f refers to the fine particulate matter, ρ is the particle mass density, which is assumed to be 1.5 g/cm^3 (Clarisse et al., 2010; Li et al., 2016).

Substituting these expressions into the above equations yields,

$$AOD_f^* = PM_f * \frac{3Q_{ext}}{4\rho r_e} = PM_f * \frac{3\kappa_{ext}}{4\pi\rho (r_g)^3 \exp(9/2\ \ln^2\ \sigma_g)} \tag{10}$$

Therefore,

$$PM_f = \frac{AOD * FMF}{PBLH * f(RH)} * \frac{4\pi\rho (r_g)^3 \exp(9/2\ \ln^2\sigma_g)}{3(3.912/VIS)} \tag{11}$$

In Eq. (11), AOD, FMF, PBLH, f(RH) and VIS are obtained from satellite and re-analysis data; ρ and σ_g are the constants, and r_g is calculated using ground-based $PM_{2.5}$ measurements. Additionally, we assumed that PM_f derived by AOD_f is equal to $PM_{2.5}$. However, the truncation diameter of AOD_f is smaller than that of $PM_{2.5}$, which could introduce errors into the retrieval (O'Neill 2003). Hence, a correction factor 0.86 was applied to minimize this bias (Li et al., 2016).

3.2. Particle aerodynamic diameter calculation

We relate Eqs. (5) and (9) to ground-level r_g in Eq. (10), deriving both $PM_{2.5}$ mass concentration and ground-level r_e simultaneously, primarily from satellite-retrieved AOD and meteorological parameters. Ground-level particle radius is purposefully preserved rather than eliminated so that it may also be retrieved, yielding additional insight relevant to understanding exposure to fine and ultrafine particulate matter. Ground-based measurements used in the estimation of r_g were not used to validate retrieved $PM_{2.5}$ mass concentrations, with details as follows.

The particle size of $PM_{2.5}$ was expressed in terms of aerodynamic diameter, d_{ae}, as per the definition of $PM_{2.5}$. To do this, first, all matched samples for each day were randomly divided into five equal size subgroups. A single subgroup was adopted as the validation sample set and the remaining four were employed to calculate particle radius (r_g) using Eq. (11). This process was iterated five times, with each of the five subgroups used exactly once for validation. The station-based daily mean particle radius was interpolated using the IDW method with 3 km spatial resolution. We masked the pixels where the corresponding AOD values were not available to reduce bias. The daily particle radius was then averaged to obtain the seasonal spatial distribution. Finally, the seasonal average geometric particle radius was used to find the equivalent aerodynamic diameter. To relate the aerodynamic diameters (d_{ae}) to the geometric diameter (d_g), the volume equivalent diameters d_e is introduced. Assuming that aerosols in the atmosphere are spherical particles, $d_e = d_g$ and $d_g = 2r_g$. Therefore, according previous studies (Raabe 1976; Hand and Kreidenweis 2002):

$$d_{ae} = d_e(\rho/\rho^*)^{1/3} = d_g(\rho/\rho^*)^{1/3} = 2r_g(\rho/\rho^*)^{1/3} \tag{12}$$

where ρ^* is the standardizing density equal to 1 g/cm^3.

3.3. Method correction and validation

There are more than 1500 VIS stations over China, which is comparable with the number of $PM_{2.5}$ sites. The $PM_{2.5}$ concentrations estimated by interpolated VIS are difficult to validate if the VIS stations are close to the PM mass monitoring sites. Therefore, the daily VIS data from the stations near the $PM_{2.5}$ monitoring stations were removed to show the extendibility of the proposed method. A leave-one-out cross validation was conducted to assess accuracy. The spatial distributions of the VIS and $PM_{2.5}$ stations are shown in Supplementary material Fig. S7.

Satellite-observed AOD values can be biased or missing due to high surface reflectance or cloud and high aerosol loading, resulting in $PM_{2.5}$ underestimation (Guo et al., 2017b; Gupta et al., 2016). A correction factor C_i calculated using Eq. (13) were adopted to correct these errors:

$$C_i = \frac{PM_{2.5,obs\_i}}{PM_{2.5,est\_i}} \tag{13}$$

where $PM_{2.5,obs\_i}$ and $PM_{2.5,est\_i}$ are the average observed and estimated $PM_{2.5}$ mass concentration at pixel *i*. The factors were extrapolated to all pixels over the study are using IDW algorithm. The final $PM_{2.5}$ estimation at annual and seasonal scale is calculated by correction factors and uncorrected estimated values.

Five metrics, including Pearson coefficient (R), root-mean-square error (RMSE), mean absolute error (MAE), mean bias error (MBE) and relative percentage error (RPE), were used to assess the retrieval bias.

$$RMSE = \sqrt{\frac{1}{N}\sum_{i=1}^{N}(est_i - obs_i)^2} \tag{14}$$

$$MAE = \frac{1}{N}\sum_{i=1}^{N}|est_i - obs_i| \tag{15}$$

$$MBE = \frac{1}{N}\sum_{i=1}^{N}(est_i - obs_i) \tag{16}$$

$$RPE = \frac{1}{N}\sum_{i=1}^{N}\left|\frac{est_i - obs_i}{obs_i}\right| \tag{17}$$

where obs_i and est_i are the observed and estimated value of sample *i*, respectively. $\bar{obs}$ and $\bar{est}$ are the average observed and estimated value. N is the number of validation samples.

4. Results

4.1. Estimation of particle size

Fig. 2 depicts the mean aerodynamic particle diameter of $PM_{2.5}$, calculated using Eq. (12). The mean particle size is larger in the northwest than in the southeast, especially in summer (Fig. 2b). The division coincides with the Heihe–Tengchong line, which is an imaginary line dividing the territory of China into western and eastern parts (Hu, 1935). The results indicate that people living in eastern China (with 43% of the area and 94% of the population in 2015) are exposed to PM with smaller diameters. Although the proportion of smaller particles in summer is higher than that in the other three seasons, the area with the largest particle size (the Taklamakan Desert) also occurred in summer. The AE in the Taklamakan Desert presents larger values in spring and summer compared with that in the other two seasons (Wang et al., 2013). Our results show a similar pattern since AE is inversely associated with particle size. The seasonal variations are also noted by previous studies (Chubarova et al., 2016; Tian et al., 2015). The statistical characteristics of the retrieved particle size are shown in Table 1 and the frequency statistics are provided in Fig. S8.

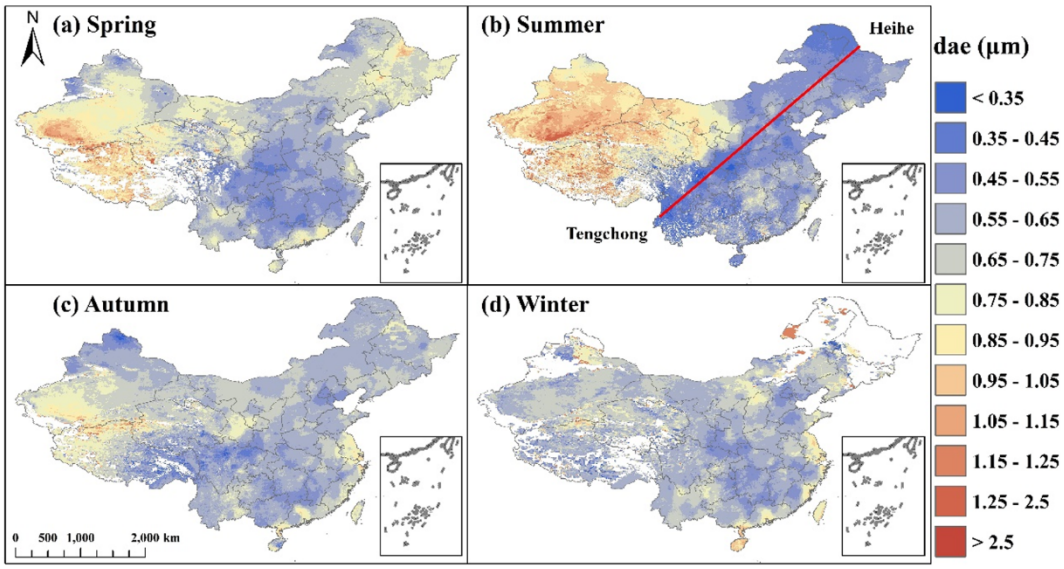

Fig. 2. Spatiotemporal distribution of aerodynamic diameters over China.

Table 1
Statistical characteristic of aerosol aerodynamic diameters (μm).

Season	Minimum	Maximum	Mean	Standard deviation	N
Spring	0.23	3.23	0.69	0.15	1,204,153
Summer	0.19	6.87	0.69	0.23	1,230,878
Autumn	0.18	4.37	0.64	0.10	1,275,501
Winter	0.20	3.60	0.65	0.11	1,042,324
Annual	0.21	2.86	0.67	0.11	1,289,860

Spring: DOY 60 ~ 149; Summer: DOY 150 ~ 241; Autumn: DOY 242 ~ 332; Winter: DOY 1 ~ 59; 333 ~ 365; DOY: Day of Year.

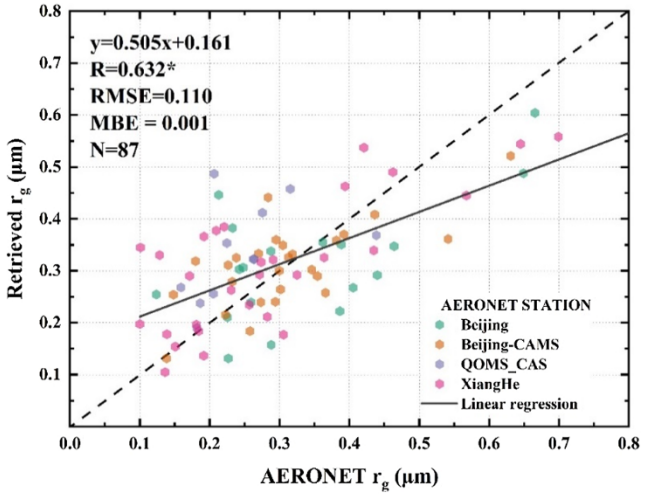

Fig. 3. Validation of satellite-retrieved and AERONET measurement-retrieved radius in 2017.

The retrieved r_g was also compared with measured values. Effective radius at four AERONET stations (Version 3 Level 2.0) in China were downloaded and calculated for validation. Although there are only 87 retrieved-measured r_g samples in total due to the availability of collocated Level 2.0 data, this is a good start for large-scale particle size estimation over land, with RMSE of 0.11 μm, which enables diverse particle size to be distinguished (Fig. 3). The relationship is statistically significant at the 0.05 significance level. However, it should be noted that the r_e obtained from AERONET is in the total atmospheric column, while the radius retrieved in our study is at ground level (Prats et al., 2011). The small, positive value of MBE in Fig. 3 shows that the ground-level radius is larger than the columnar value, which is consistent with the evidence that the aerosol radius decreases slightly with altitude (Baars et al., 2012).

4.2. Temporal variation of retrieved $PM_{2.5}$

The monthly variation of measured and estimated $PM_{2.5}$ concentrations across China is shown in Fig. 4a. As shown, heavily polluted periods are more likely to occur between Jan-Feb and Nov-Dec when heating systems are operating in Northern China. The $PM_{2.5}$ concentration differences among stations in Mar-Sep (spring and summer) are lower than those in other months. These results are consistent with the seasonal distribution of $PM_{2.5}$ (Fig. S9). Summertime has the lowest $PM_{2.5}$, with seasonal means of 27.38 μg/m^3, while winter is the most polluted season with mean concentrations equal to 58.60 μg/m^3 in 2017. The highest RMSE also occurred in winter, followed by autumn, spring and summer (Fig. 4b). The monthly variation of RPE is stable, with an average of 31.32%. Additionally, the performance of the proposed method is also evaluated at the seasonal scale (Table 2). The highest correlation coefficient is 0.91 in winter, with RMSE of 20.02 μg/m^3 and RPE of 27.54%.

Based on the spatial pattern of annual $PM_{2.5}$ concentrations, five regions, including Beijing-Tianjin-Hebei Metropolitan region (BTH), Yangtze River Delta (YRD), Pearl River Delta (PRD), Sichuan Basin (SB) and Taklamakan Desert (TD), were selected to present regional monthly variation (Fig. 5). The overall variations among these five areas are similar with that across China and the highest $PM_{2.5}$ values were observed in the BTH region.

4.3. Spatial distribution of retrieved $PM_{2.5}$

The annual mean of satellite-retrieved $PM_{2.5}$ concentrations over China was estimated to be 46.88 μg/m^3. The spatial pattern of the retrieved $PM_{2.5}$ appears to be consistent with that of ground measurements and other studies (van Donkelaar et al., 2010). The BTH region experienced high $PM_{2.5}$ exposures in 2017, with concentrations higher than 55 μg/m^3. Among the four hotspots highlighted in Fig. 6, the BTH region had the highest annual mean concentrations, followed by the SB, the YRD and the PRD region. Except for the above four regions, high $PM_{2.5}$ levels were also observed in the Taklamakan Desert.

The evaluation of uncorrected estimates is shown in Fig. S10 and

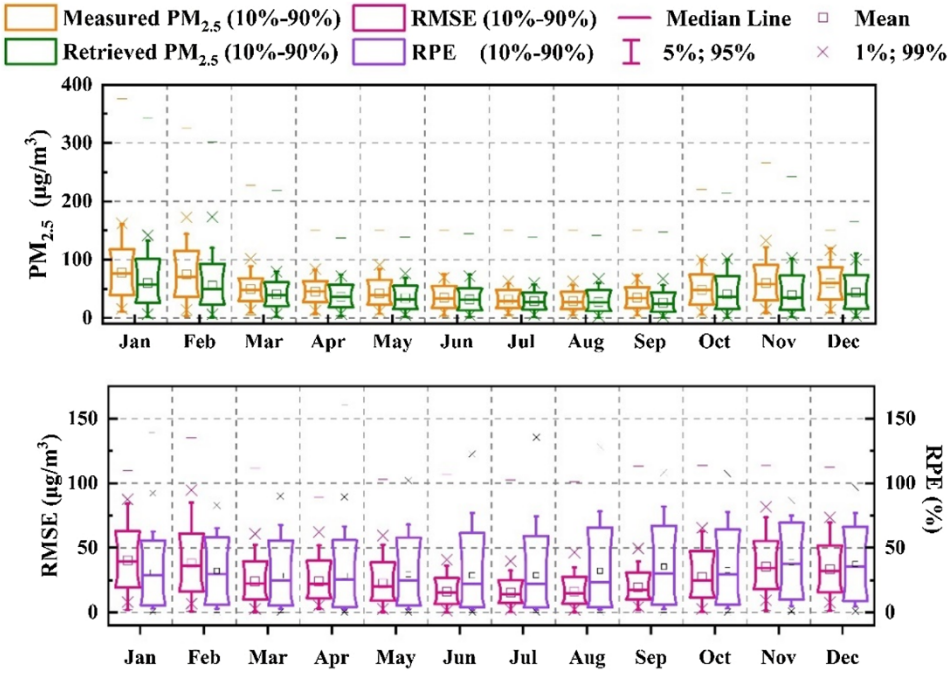

Fig. 4. Temporal variation of (a) measured and estimated $PM_{2.5}$ concentrations, and (b) RMSE and RPE across China.

Table 2
Correlation between seasonal-mean retrieved and in-situ $PM_{2.5}$ concentration.

Season	R	RMSE (μg/m^3)	RPE	N
Spring	0.77	12.87	22.72%	1255
Summer	0.72	9.42	22.91%	1245
Autumn	0.83	14.83	26.68%	1242
Winter	0.91	20.02	27.54%	1193

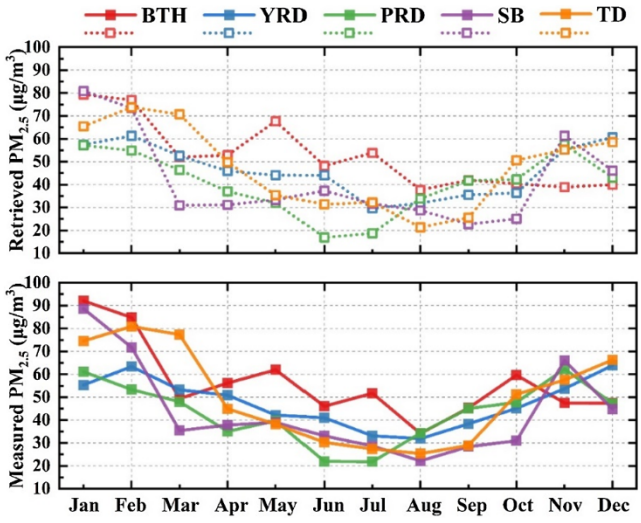

Fig. 5. Monthly variation of retrieved and measured $PM_{2.5}$ concentrations in the BTH, YRD, PRD, SB and TD region.

Fig. S11, which illustrates the underestimation of $PM_{2.5}$ mass concentration. The possible reason is that high aerosol loading might be misclassified into cloud, leading to missing values in satellite images under severe air pollution. Therefore, $PM_{2.5}$ estimates were improved with correction factors and evaluated using ground measurements. The promising accuracy for annual (R = 0.82, RMSE = 9.25 μg/m^3, MAE = 6.98 μg/m^3, MBE = −1.98 μg/m^3, RPE = 17.69%, N = 1270) and seasonal (R = 0.81, RMSE = 12.13 μg/m^3, MAE = 9.35 μg/m^3, MBE = -0.36 μg/m^3, RPE = 24.23%, N = 4932) means are reported in Fig. 7. The bias of the corrected results might be due to the limited spatio-temporal coverage and uncertainties of input data. Since DT has limited capability of bright surface AOD retrieval, the AOD from 10 km DB could cause uncertainty due to spatial heterogeneity. Meanwhile, sparsely distributed monitoring sites and reduced satellite coverage affected the $PM_{2.5}$ retrieval by reducing the accuracy of the retrieved particle radius.

5. Discussion

An optical-mass conversion algorithm was established to quantify $PM_{2.5}$ concentrations using satellite-observed data. The particle diameters and $PM_{2.5}$ concentrations were estimated and validated over China. Our aerosol diameter results show that the mean particle size in eastern China was smaller than in other regions, which might be attributed to differences in topography, meteorology, land use, and population density, affecting the properties of emitted aerosols as well as their fate and transport. According to previous studies (Huang and Luo 2008; Qian and Liu 2018; Wang et al., 2004), due to land use and topography in China, aerosol loading to the east of the Heihe-Tengchong line is high, which is likely attributed to human activity. Values in the west are relatively low, which might be influenced by natural sources (such as sand and dust). These findings are consistent with our size results. This observed pattern does show some seasonality, though 90% of pixels have diameters less than 1 μm throughout all seasons. Across the domain, particle sizes were generally larger in the spring and summer, and smaller in the autumn and winter. This seasonality may be attributed to variations in the sources, fate, and transport of fine particulate matter (Zhang et al., 2013).

A similar spatial pattern was also observed in mass concentration. The heavy pollution in the BTH region is likely attributable to unfavorable topography, regional transport and anthropogenic activities associated with urbanization and industrialization (such as fossil fuel consumption) (He and Huang 2018; Zheng et al., 2015). The pollution in the SB region was likely due to relatively low elevations and stagnant air circulation (You et al., 2016) and the polluted air in the TD region was mainly attributed to dust and sand (Ma et al., 2014). In the PRD,

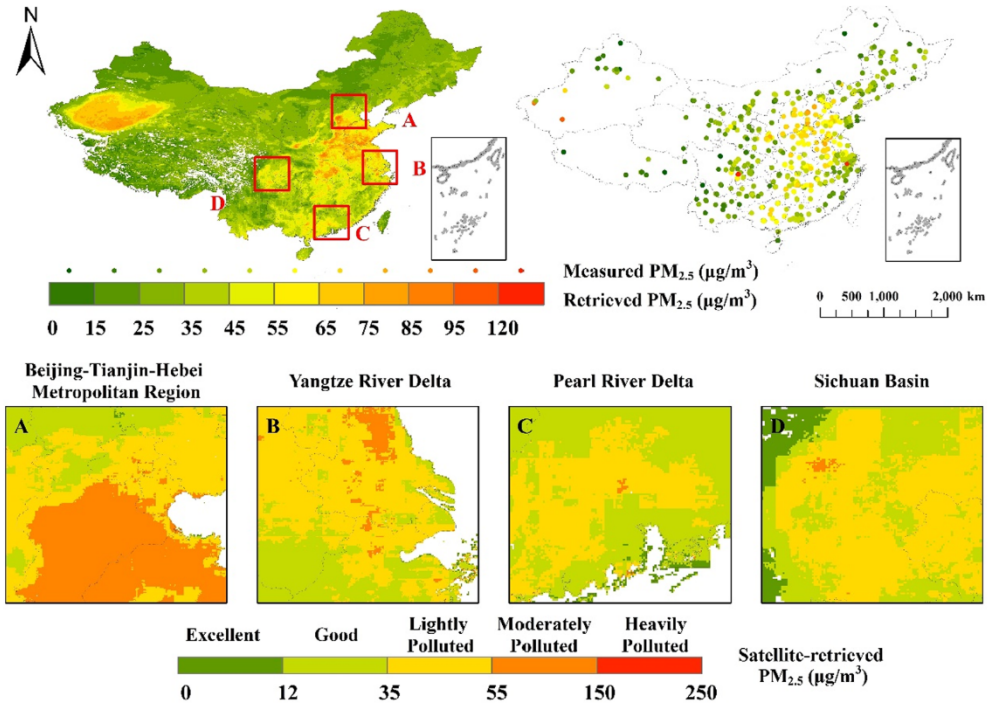

Fig. 6. Spatial distribution of annual mean satellite-retrieved and ground-based $PM_{2.5}$ concentrations with four hotspots.

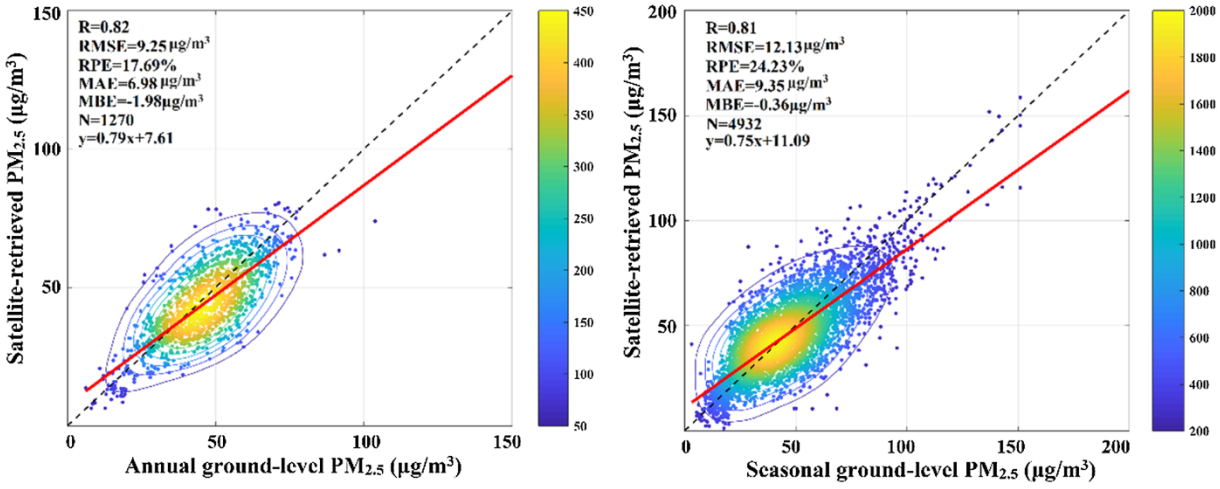

Fig. 7. Validation of $PM_{2.5}$ retrievals over China at annual and seasonal scales.

$PM_{2.5}$ concentrations were predominantly rated "lightly polluted" or "good", though some coastal regions showed "excellent" levels, which could indicate an underestimation in coastal areas, where surface reflectance can be more challenging to characterize (Anderson et al., 2013). Temporally, the highest $PM_{2.5}$ concentrations occurred in winter while summer had the lowest concentrations. Heating-related emissions and adverse weather are two possible reasons for higher pollution in winter (He and Huang, 2018; Ma et al., 2014). The $PM_{2.5}$ retrievals were validated at 1270 stations in China in more than 350 available days, with acceptable correlation between annual-mean retrieved and measured $PM_{2.5}$ concentrations. These results provide evidence to support the reliability of this conversion algorithm for retrieving ground $PM_{2.5}$ concentrations with an explicit mechanism.

Compared with other retrieval methods (Lin et al., 2015; Zhang and Li, 2015), the AOD-$PM_{2.5}$ relationship in our study builds upon aerosol microphysical characteristics without introducing regional fitting parameters, making it easier to apply across spatial and temporal domains. However, the performance of this method is affected by two main sources: input data and retrieval assumptions. Spatial heterogeneity affects the processes of data retrieval, gap-filling and interpolation, which could lead to random and systematic errors. Although MODIS AOD is one of the most widely used and well-validated products for $PM_{2.5}$ retrieval, biases remain because of the retrieval algorithm and cloud contamination. High aerosol loading might be misclassified into cloud, leading to missing values during periods of severe haze. Meanwhile, the input data might be also biased due to algorithm errors, interpolation errors and systematic errors. For example, the separation of MODIS retrieval algorithms over land and ocean may lead to inaccuracy over pixels containing land and ocean (Anderson et al., 2013). Consistent with the satellite transit time, the retrieved $PM_{2.5}$ in this study corresponds to values between 10:00am and 14:00 pm instead of a daily average. This potential bias should be addressed prior to use as a daily average, for example, in health studies.

In addition to the uncertainty caused by input data, the retrieval method in our studies could also introduce errors. Although particle radius could be determined with the model, high precision was difficult

to achieve with the limited ground-based measurements. Compared to the observed data acquired from AERONET, the relative error of particle radius in this study is approximately 7%; however, this needs to be further tested, especially in the regions where verification sites are limited. It is more problematic to adopt an empirical constant as the radius due to the spatiotemporal variance of aerosols. Therefore, future work should seek to address this using the micro-properties of aerosols from a mechanistic prospective at large scale. Furthermore, assumptions used in our study could also introduce bias. Previous studies have indicated that particle density and distribution vary in the columnar atmosphere (Liu et al., 2015; Yan et al., 2017b). The assumptions of constant values for ρ and σ_g and uniform vertical distribution can lead to an error of 18% and 16.6%, respectively (Li et al., 2016; Zhang and Li, 2015). The total uncertainty of related to assumptions in our optical-mass conversion algorithm is approximately 29%. Additionally, there are several other factors regarded to be causally associated with $PM_{2.5}$ concentration and the mechanism of how these parameters impact observations was not fully understood, which offers a fertile field for study.

6. Conclusion

A satellite-based optical-mass conversion algorithm was established in this study to quantify $PM_{2.5}$ mass concentrations based on aerosol microphysical characteristics, which can simultaneously estimate particle size. The estimated particle radius was quantified against the available ground-based columnar measurements, with RMSE = 0.11 μm. The validation result shows that the ground-level radius is slightly larger than the corresponding columnar value on average, which is consistent with the findings that aerosol radius decreases slightly with altitude. The spatial distribution shows that particle diameters in eastern China are smaller than those in other regions, which might be due to differences in features such as topography, meteorology, land use and population density in China. Additionally, the estimated $PM_{2.5}$ concentrations were corrected and validated using ground measurements at annual and seasonal scales, with RMSE = 9.25 μg/m^3, MAE = 6.98 μg/m^3, MBE = −1.98 μg/m^3, RPE = 17.69% (N = 1270). The spatiotemporal distribution of satellite-retrieved $PM_{2.5}$ agrees with the in-situ data and findings from previous studies. Highly polluted periods are more likely to occur between Jan-Feb and Nov-Dec, while summertime has the lowest $PM_{2.5}$ concentrations. Spatially, the BTH regions experienced a higher $PM_{2.5}$ pollution compared with other major metropolitan areas. This approach builds on previous optical-mass studies by avoiding regional fitting and retrieving particle size. It can thus potentially fill an important gap in estimating exposure to ultrafine particles (which are thought to be more toxic, but lack of large-scale, high-resolution measurements). Further work is needed to increase the accuracy of this method, which would benefit from the improvement of sensors and algorithms.

Acknowledgements

The authors would like to thank NASA MODIS, AERONET and UCAR for their publicly available data. The first author acknowledges the China Scholarship Council for their support via a doctoral scholarship (No. 201706400072).

Declaration of Competing Interest

The authors declare no conflict of interest.

Appendix A. Supplementary material

Supplementary data to this article can be found online at https://doi.org/10.1016/j.isprsjprs.2019.10.010.

References

Anderson, J.C., Wang, J., Zeng, J., Leptoukh, G., Petrenko, M., Ichoku, C., Hu, C., 2013. Long-term statistical assessment of Aqua-MODIS aerosol optical depth over coastal regions: bias characteristics and uncertainty sources. Tell. B: Chem. Phys. Meteorol. 65 (1), 20805.
Baars, H., Ansmann, A., Althausen, D., Engelmann, R., Heese, B., Müller, D., Artaxo, P., Paixao, M., Pauliquevis, T., Souza, R., 2012. Aerosol profiling with lidar in the Amazon Basin during the wet and dry season. J. Geophys. Res.: Atmos. 117, D21.
Ceca, L.S.D., Ferreyra, M.F.G., Lyapustin, A., Chudnovsky, A., Otero, L., Carreras, H., Barnaba, F., 2018. Satellite-based view of the aerosol spatial and temporal variability in the Cordoba region (Argentina) using over ten years of high-resolution data. ISPRS J. of Photo. Rem. Sen. 145, 250–267.
Chen, G., Li, S., Zhang, Y., Zhang, W., Li, D., Wei, X., He, Y., Bell, M.L., Williams, G., Marks, G.B., 2017. Effects of ambient PM 1 air pollution on daily emergency hospital visits in China: an epidemiological study. Lancet Planet. Health 1 (6), e221–e229.
Chen, J., Zhao, C.S., Ma, N., Yan, P., 2014. Aerosol hygroscopicity parameter derived from the light scattering enhancement factor measurements in the North China Plain. Atmos. Chem. Phys. 14 (15), 8105–8118.
Chen, L., Liu, C., Zou, R., Yang, M., Zhang, Z., 2016. Experimental examination of effectiveness of vegetation as bio-filter of particulate matters in the urban environment. Environ. Pollut. 208, 198–208.
China, M.E.P., 2012. Ambient Air Quality Standards. GB 3095–2012. China Environmental Science Press, Beijing.
Chubarova, N., Poliukhov, A., Gorlova, I., 2016. Long-term variability of aerosol optical thickness in Eastern Europe over 2001–2014 according to the measurements at the Moscow MSU MO AERONET site with additional cloud and NO 2 correction. Atmos. Meas. Tech. 9 (2), 313.
Clarisse, L., Hurtmans, D., Prata, A.J., Karagulian, F., Clerbaux, C., De Mazière, M., Coheur, P.-F., 2010. Retrieving radius, concentration, optical depth, and mass of different types of aerosols from high-resolution infrared nadir spectra. Appl. Opt. 49 (19), 3713–3722.
Cohen, A.J., Brauer, M., Burnett, R., Anderson, H.R., Frostad, J., Estep, K., Balakrishnan, K., Brunekreef, B., Dandona, L., Dandona, R., 2017. Estimates and 25-year trends of the global burden of disease attributable to ambient air pollution: an analysis of data from the global burden of diseases study 2015. Lancet 389 (10082), 1907–1918.
de Hartog, J.J., Lanki, T., Timonen, K.L., Hoek, G., Janssen, N.A., Ibald-Mulli, A., Peters, A., Heinrich, J., Tarkiainen, T.H., van Grieken, R., 2009. Associations between PM2. 5 and heart rate variability are modified by particle composition and beta-blocker use in patients with coronary heart disease. Environ. Health Perspect. 117 (1), 105.
Di, Q., Koutrakis, P., Schwartz, J., 2016. A hybrid prediction model for PM2. 5 mass and components using a chemical transport model and land use regression. Atmos. Environ. 131, 390–399.
Eck, T.F., Holben, B.N., Reid, J.S., Dubovik, O., Smirnov, A., O'Neill, N.T., Slutsker, I., Kinne, S., 1999. Wavelength dependence of the optical depth of biomass burning, urban, and desert dust aerosols. J. Geophys. Res.: Atmos. 104 (D24), 31333–31349.
Guo, J., Xia, F., Zhang, Y., Liu, H., Li, J., Lou, M., He, J., Yan, Y., Wang, F., Min, M., Zhai, P., 2017a. Impact of diurnal variability and meteorological factors on the PM2.5 - AOD relationship: implications for PM2.5 remote sensing. Environ. Pollut. 221, 94–104.
Guo, Y., Tang, Q., Gong, D.-Y., Zhang, Z., 2017b. Estimating ground-level PM 2.5 concentrations in Beijing using a satellite-based geographically and temporally weighted regression model. Rem. Sens. Environ. 198, 140–149.
Gupta, P., Christopher, S.A., 2009. Particulate matter air quality assessment using integrated surface, satellite, and meteorological products: 2. A neural network approach. J. Geophys. Res.: Atmos. 114, D20.
Gupta, P., Levy, R.C., Mattoo, S., Remer, L.A., Munchak, L.A., 2016. A surface reflectance scheme for retrieving aerosol optical depth over urban surfaces in MODIS Dark Target retrieval algorithm. Atmos. Meas. Tech. 9 (7), 3293–3308.
Han, L., Zhou, W., Li, W., 2016. Fine particulate (PM2.5) dynamics during rapid urbanization in Beijing, 1973–2013. Sci. Report 6, 23604.
Hand, J.L., Kreidenweis, S.M., 2002. A new method for retrieving particle refractive index and effective density from aerosol size distribution data. Aerosol Sci. Technol. 36 (10), 1012–1026.
Hansen, J.E., Travis, L.D., 1974. Light scattering in planetary atmospheres. Space Sci. Rev. 16 (4), 527–610.
Hao, Y., Liu, Y.-M., 2016. The influential factors of urban PM2. 5 concentrations in China: a spatial econometric analysis. J. Cleaner Prod. 112, 1443–1453.
He, Q., Huang, B., 2018. Satellite-based mapping of daily high-resolution ground PM 2.5 in China via space-time regression modeling. Remote Sens. Environ. 206, 72–83.
Hobbs, P.V., Radke, L.F., Lyons, J.H., Ferek, R.J., Coffman, D.J., Casadevall, T.J., 1991. Airborne measurements of particle and gas emissions from the 1990 volcanic eruptions of mount redoubt. J. Geophys. Res.: Atmos. 96 (D10), 18735–18752.
Hofmann, D., Rosen, J.M., 1983. Sulfuric acid droplet formation and growth in the stratosphere after the 1982 eruption of El Chichon. Science 222 (4621), 325–327.
Hsu, N., Jeong, M.J., Bettenhausen, C., Sayer, A., Hansell, R., Seftor, C., Huang, J., Tsay, S.C., 2013. Enhanced Deep Blue aerosol retrieval algorithm: the second generation. J. Geophys. Res.: Atmos. 118 (16), 9296–9315.
Hu, H.Y., 1935. The Distribution of Population in China, With Statistics and Maps. Acta Geographica Sinica 2 (2), 33–74.
Hu, X., Waller, L.A., Lyapustin, A., Wang, Y., Al-Hamdan, M.Z., Crosson, W.L., Estes Jr, M.G., Estes, S.M., Quattrochi, D.A., Puttaswamy, S.J., 2014. Estimating ground-level PM2. 5 concentrations in the Southeastern United States using MAIAC AOD retrievals and a two-stage model. Remote Sens. Environ. 140, 220–232.
Huang, Y., Luo, X., 2008. Geography in China. Reshaping Economic Geography East Asia 196.
Junge, C., 1955. The size distribution and aging of natural aerosols as determined from electrical and optical data on the atmosphere. J. Meteorol. 12 (1), 13–25.
King, M.D., Byrne, D.M., 1976. A method for inferring total ozone content from the spectral variation of total optical depth obtained with a solar radiometer. J. Atmos.

Sci. 33 (11), 2242–2251.
Koelemeijer, R.B.A., Homan, C.D., Matthijsen, J., 2006. Comparison of spatial and temporal variations of aerosol optical thickness and particulate matter over Europe. Atmos. Environ. 40 (27), 5304–5315.
Koschmieder, H., 1925. Theorie der horizontalen Sichtweite. Physik der freien Atmosphäre 12, 171.
Kumar, N., Chu, A., Foster, A., 2007. An empirical relationship between PM2. 5 and aerosol optical depth in Delhi Metropolitan. Atmos. Environ. 41 (21), 4492–4503.
Lee, H., Liu, Y., Coull, B., Schwartz, J., Koutrakis, P., 2011. A novel calibration approach of MODIS AOD data to predict PM2. 5 concentrations. Atmos. Chem. Phys. 11 (15), 7991.
Levy, R.C., Remer, L.A., Mattoo, S., Vermote, E.F., Kaufman, Y.J., 2007. Second-generation operational algorithm: Retrieval of aerosol properties over land from inversion of Moderate Resolution Imaging Spectroradiometer spectral reflectance. J. Geophy. Res.: Atmos. 112 (D13), 211.
Li, X., Zhang, C., Li, W., Liu, K., 2017. Evaluating the Use of DMSP/OLS Nighttime Light Imagery in Predicting PM2.5 Concentrations in the Northeastern United States. Remote Sensing 9 (6), 620.
Li, Y., Chen, Q., Zhao, H., Wang, L., Tao, R., 2015. Variations in PM10, PM2. 5 and PM1. 0 in an urban area of the Sichuan Basin and their relation to meteorological factors. Atmosphere 6 (1), 150–163.
Li, Z., Zhang, Y., Shao, J., Li, B., Hong, J., Liu, D., Li, D., Wei, P., Li, W., Li, L., 2016. Remote sensing of atmospheric particulate mass of dry PM2. 5 near the ground: Method validation using ground-based measurements. Remote Sens. Environ. 173, 59–68.
Lin, C., Li, Y., Yuan, Z., Lau, A.K.H., Li, C., Fung, J.C.H., 2015. Using satellite remote sensing data to estimate the high-resolution distribution of ground-level PM2.5. Remote Sens. Environ. 156, 117–128.
Lin, G., Fu, J., Jiang, D., Hu, W., Dong, D., Huang, Y., Zhao, M., 2013. Spatio-temporal variation of PM2. 5 concentrations and their relationship with geographic and socioeconomic factors in China. Int. J. Environ. Res. Public Health 11 (1), 173–186.
Li, L., Yang, J., Wang, Y., 2014. An improved dark object method to retrieve 500m-resolution AOT (Aerosol Optical Thickness) image from MODIS data: A case study in the Pearl River Delta area, China. ISPRS J. Photo. Rem. Sen. 89, 1–12.
Liu, X., Cheng, Y., Zhang, Y., Jung, J., Sugimoto, N., Chang, S.-Y., Kim, Y.J., Fan, S., Zeng, L., 2008. Influences of relative humidity and particle chemical composition on aerosol scattering properties during the 2006 PRD campaign. Atmos. Environ. 42 (7), 1525–1536.
Liu, Y., He, K., Li, S., Wang, Z., Christiani, D.C., Koutrakis, P., 2012. A statistical model to evaluate the effectiveness of PM2. 5 emissions control during the Beijing 2008 Olympic Games. Environ. Int. 44, 100–105.
Liu, Y., Paciorek, C.J., Koutrakis, P., 2009. Estimating regional spatial and temporal variability of PM2. 5 concentrations using satellite data, meteorology, and land use information. Environ. Health Perspect. 117 (6), 886.
Liu, Y., Sarnat, J.A., Kilaru, V., Jacob, D.J., Koutrakis, P., 2005. Estimating ground-level PM2. 5 in the eastern United States using satellite remote sensing. Environ. Sci. Technol. 39 (9), 3269–3278.
Liu, Z., Hu, B., Ji, D., Wang, Y., Wang, M., Wang, Y., 2015. Diurnal and seasonal variation of the PM2. 5 apparent particle density in Beijing, China. Atmos. Environ. 120, 328–338.
Luo, J., Du, P., Samat, A., Xia, J., Che, M., Xue, Z., 2017. Spatiotemporal pattern of PM2.5 concentrations in mainland china and analysis of its influencing factors using geographically weighted regression. Scientific Report 7, 40607.
Lyapustin, A., Wang, Y., Korkin, S., Huang, D.J.A.M.T., 2018. MODIS Collection 6 MAIAC algorithm. Atmos. Meas. Tech. 11 (10), 5741–5765.
Ma, L., Liu, Y., Zhang, X., Ye, Y., Yin, G., Johnson, B.A., 2019. Deep learning in remote sensing applications: A meta-analysis and review. ISPRS J. Photogramm. Remote Sens. 152, 166–177.
Ma, Z., Hu, X., Huang, L., Bi, J., Liu, Y., 2014. Estimating ground-level PM2.5 in China using satellite remote sensing. Environ. Sci. Technol. 48 (13), 7436–7444.
Ma, Z., Hu, X., Sayer, A.M., Levy, R., Zhang, Q., Xue, Y., Tong, S., Bi, J., Huang, L., Liu, Y., 2016. Satellite-Based Spatiotemporal Trends in PM2.5 Concentrations: China, 2004-2013. Environ. Health Perspect. 124 (2), 184–192.
O'Neill, N.T., 2003. Spectral discrimination of coarse and fine mode optical depth. J. Geophys. Res. 108 (D17), 4559.
Ostro, B., Hu, J., Goldberg, D., Reynolds, P., Hertz, A., Bernstein, L., Kleeman, M.J., 2015. Associations of mortality with long-term exposures to fine and ultrafine particles, species and sources: results from the California Teachers Study Cohort. Environ. Health Perspect. 123 (6), 549.
Pope, C.A., Ezzati, M., Cannon, J.B., Allen, R.T., Jerrett, M., Burnett, R.T., 2018. Mortality risk and PM 2.5 air pollution in the USA: an analysis of a national prospective cohort. Air Qual. Atmos. Health 11, 1–8.
Prats, N., Cachorro, V., Berjón, A., Toledano, C., De Frutos, A., 2011. Column-integrated aerosol microphysical properties from AERONET Sun photometer over southwestern Spain. Atmos. Chem. Phys. 11 (24), 12535–12547.
Qian, J., Liu, C., 2018. Distributions and changes of aerosol optical depth on both sides of HU Huanyong Line and the response to land use and land cover. Acta Scientiae Circumstantiae 38, 752–760.
Raabe, O.G., 1976. Aerosol aerodynamic size conventions for inertia! sampler calibration. J. Air Poll. Control Assoc. 26 (9), 856–860.
Reid, J.S., Jonsson, H.H., Maring, H.B., Smirnov, A., Savoie, D.L., Cliff, S.S., Reid, E.A., Livingston, J.M., Meier, M.M., Dubovik, O., 2003. Comparison of size and morphological measurements of coarse mode dust particles from Africa. J. Geophys. Res.: Atmos. 108 (D19), 8593.
Remer, L., Mattoo, S., Levy, R., Munchak, L., 2013. MODIS 3 km aerosol product: algorithm and global perspective. Atmos. Meas. Tech. 6, 1829.
Sacks, J.D., Stanek, L.W., Luben, T.J., Johns, D.O., Buckley, B.J., Brown, J.S., Ross, M., 2011. Particulate matter–induced health effects: who is susceptible? Environ. Health Perspect. 119 (4), 446–454.
Samoli, E., Andersen, Z.J., Katsouyanni, K., Hennig, F., Kuhlbusch, T.A., Bellander, T., Cattani, G., Cyrys, J., Forastiere, F., Jacquemin, B., 2016. Exposure to ultrafine particles and respiratory hospitalisations in five European cities. Eur. Respir. J. 48 (3), 674–682.
Schuster, G.L., Dubovik, O., Holben, B.N., 2006. Angstrom exponent and bimodal aerosol size distributions. J. Geophys. Res.-Atmos. 111 (D7). https://doi.org/10.1029/2005JD006328.
Stafoggia, M., Schneider, A., Cyrys, J., Samoli, E., Andersen, Z.J., Bedada, G.B., Bellander, T., Cattani, G., Eleftheriadis, K., Faustini, A., 2017. Association between short-term exposure to ultrafine particles and mortality in eight European urban areas. Epidemiology 28 (2), 172–180.
Steele, H.M., Eldering, A., Lumpe, J.D., 2006. Simulations of the accuracy in retrieving stratospheric aerosol effective radius, composition, and loading from infrared spectral transmission measurements. Appl. Opt. 45 (9), 2014–2027.
Steyn, D.G., Galmarini, S., 2008. Evaluating the predictive and explanatory value of atmospheric numerical models: between relativism and objectivism. Open Atmos. Sci. J. 2 (1), 38–45.
Tang, Y., Chai, T., Pan, L., Lee, P., Tong, D., Kim, H.C., Chen, W., 2015. Using optimal interpolation to assimilate surface measurements and satellite AOD for ozone and PM2. 5: A case study for July 2011. J. Air Waste Manag. Assoc. 65 (10), 1206–1216.
Tian, P., Cao, X., Zhang, L., Wang, H., Shi, J., Huang, Z., Zhou, T., Liu, H., 2015. Observation and simulation study of atmospheric aerosol nonsphericity over the Loess Plateau in northwest China. Atmos. Environ. 117, 212–219.
van Donkelaar, A., Martin, R.V., Brauer, M., Kahn, R., Levy, R., Verduzco, C., Villeneuve, P.J., 2010. Global estimates of ambient fine particulate matter concentrations from satellite-based aerosol optical depth: development and application. Environ. Health Perspect. 118 (6), 847–855.
van Donkelaar, A., Martin, R.V., Spurr, R.J., Burnett, R.T., 2015. High-resolution satellite-derived PM2.5 from optimal estimation and geographically weighted regression over North America. Environ. Sci. Technol. 49 (17), 10482–10491.
Wang, H., Zhang, L., Cao, X., Zhang, Z., Liang, J., 2013. A-Train satellite measurements of dust aerosol distributions over northern China. J. Quant. Spectrosc. Radiat. Transfer 122, 170–179.
Wang, X., Dong, Z., Zhang, J., Liu, L., 2004. Modern dust storms in China: an overview. J. Arid Environ. 58 (4), 559–574.
Yan, X., Li, Z., Luo, N., Shi, W., Zhao, W., Yang, X., Liang, C., Zhang, F., Cribb, M.J.R.S.o.E., 2019. An improved algorithm for retrieving the fine-mode fraction of aerosol optical thickness. Part 2: Application and validation in Asia. Remote Sens. Environ. 222, 90–103.
Yan, X., Li, Z., Shi, W., Luo, N., Wu, T., Zhao, W., 2017a. An improved algorithm for retrieving the fine-mode fraction of aerosol optical thickness, part 1: Algorithm development. Remote Sens. Environ. 192, 87–97.
Yan, X., Shi, W., Li, Z., Li, Z., Luo, N., Zhao, W., Wang, H., Yu, X., 2017b. Satellite-based PM 2.5 estimation using fine-mode aerosol optical thickness over China. Atmos. Environ. 170, 290–302.
Yao, F., Wu, J., Li, W., Peng, J., 2019. A spatially structured adaptive two-stage model for retrieving ground-level PM2.5 concentrations from VIIRS AOD in China. ISPRS J. Photo. Rem. Sen. 151, 263–276.
Yang, J., Hu, M., 2018. Filling the missing data gaps of daily MODIS AOD using spatio-temporal interpolation. Sci. Total Environ. 633, 677–683.
Yang, X., Zheng, Y., Geng, G., Liu, H., Man, H., Lv, Z., He, K., de Hoogh, K., 2017. Development of PM2.5 and NO2 models in a LUR framework incorporating satellite remote sensing and air quality model data in Pearl River Delta region, China. Environtal Pollution 226, 143–153.
You, W., Zang, Z., Pan, X., Zhang, L., Chen, D., 2015. Estimating PM2.5 in Xi'an, China using aerosol optical depth: a comparison between the MODIS and MISR retrieval models. Sci. Total Environ. 505, 1156–1165.
You, W., Zang, Z., Zhang, L., Li, Y., Pan, X., Wang, W., 2016. National-scale estimates of ground-level PM2.5 concentration in China using geographically weighted regression based on 3 km resolution MODIS AOD. Remote Sensing 8 (3). https://doi.org/10.3390/rs8030184.
Zhang, C., Ni, Z., Ni, L., 2015a. Multifractal detrended cross-correlation analysis between PM2. 5 and meteorological factors. Physica A 438, 114–123.
Zhang, L., Sun, J.Y., Shen, X.J., Zhang, Y.M., Che, H., Ma, Q.L., Zhang, Y.W., Zhang, X.Y., Ogren, J.A., 2015b. Observations of relative humidity effects on aerosol light scattering in the Yangtze River Delta of China. Atmos. Chem. Phys. 15 (14), 8439–8454.
Zhang, R., Jing, J., Tao, J., Hsu, S.-C., Wang, G., Cao, J., Lee, C.S.L., Zhu, L., Chen, Z., Zhao, Y., Shen, Z., 2013. Chemical characterization and source apportionment of $PM_{2.5}$ in Beijing: seasonal perspective. Atmos. Chem. Phys. 13, 7053–7074. https://doi.org/10.5194/acp-13-7053-2013.
Zhang, Y., Li, Z., 2015. Remote sensing of atmospheric fine particulate matter (PM2.5) mass concentration near the ground from satellite observation. Remote Sens. Environ. 160, 252–262.
Zhao, X., Shi, H., Yu, H., Yang, P., 2016. Inversion of nighttime PM2.5 mass concentration in Beijing based on the VIIRS day-night band. Atmosphere 7 (10), 136.
Zheng, G., Duan, F., Su, H., Ma, Y., Cheng, Y., Zheng, B., Zhang, Q., Huang, T., Kimoto, T., Chang, D.J.A.C., 2015. Physics Exploring the severe winter haze in Beijing: the impact of synoptic weather, regional transport and heterogeneous reactions. Atmos. Chem. Phys. 15 (6), 2969–2983.